Retrieval of Temperature and Moisture Profiles From AMSU-A and AMSU-B Measurements

Philip W. Rosenkranz, *Fellow, IEEE*

***Abstract*—The NOAA-15 weather satellite carries the Advanced Microwave Sounding Units-A and -B (AMSU-A, AMSU-B) which measure thermal emission from an atmospheric oxygen band, two water lines, and several window frequencies. An iterated minimum-variance algorithm retrieves profiles of temperature and humidity in the atmosphere from this data. Relative humidity is converted into absolute humidity with use of the retrieved temperature profile. Two important issues in the retrieval problem are modeling of the surface and clouds. An *a priori* surface emissivity is computed on the basis of a preliminary classification, and the surface brightness spectrum is subsequently adjusted simultaneously with the moisture profile retrieval. Cloud liquid water is constrained by a condensation model that uses an extended definition of relative humidity as a parameter.**

I. Introduction

THE NOAA-15 satellite, launched in 1998, carries the first models of two new instruments, AMSU-A and AMSU-B. These instruments were designed to be used together for sounding of atmospheric temperature and moisture profiles. They measure microwave thermal emission from the atmosphere in the oxygen band from 50–58 GHz, the two water lines at 22 and 183 GHz, and several windows between the lines. Channel frequencies and passband characteristics are given in Table I. Other characteristics of these instruments are given in [1]–[4].

Unfortunately, the AMSU-B on NOAA-15 suffered interference from transmitters on the spacecraft from launch until October 1999, when the transmitters which caused most of the interference were shut down. That problem was avoided in this paper by use of data from a test on June 22, 1998, during which the transmitters were off. Future AMSU-B units will have improved shielding.

The retrieval algorithm described here is being developed for use with similar instruments that will be flown on the Aqua spacecraft of NASA's Earth Observing System (EOS). It is intended to provide the starting point for cloud-clearing of infrared measurements and a subsequent combined infrared-microwave retrieval. The algorithm draws on retrieval methods described in [14]–[18]. A Bayesian approach is taken here with a model for the observed system (atmosphere and surface) which has sufficient degrees of freedom to reproduce the brightness temperatures. *A priori* statistics are required for the parameters that characterize the state of the system. However, statistical correlations between temperature and relative humidity are *not* allowed to influence the retrieved profiles. Temperature is retrieved from the oxygen-band channels 4–14 and moisture and surface parameters from the water-vapor and window channels. Hence only radiative-transfer influences (e.g., water-vapor continuum absorption and surface emissivity in the oxygen band) link different parameters in the retrieval.

Rieder and Kirchengast [19] have discussed some of the advantages and limitations of Bayesian algorithms and English [20] has presented an error analysis of simulated retrievals using AMSU-A and -B frequencies. Perhaps more crucial than the method used to obtain a solution, however, is the modeling of the observation process. The need to impose some degree of regularity on (for example) surface emissivity is a consequence of ill-conditioning of the remote sensing problem. While on the one hand it would be nonphysical to set surface emissivity equal at all frequencies, on the other hand, the degrees of freedom in the system would outnumber available measurements if emissivities at different frequencies were totally independent.

TABLE I
AMSU-A/B Channel Characteristics

Channel No.	Passband center frequencies (MHz)	Passband widths (MHz)	Sensitivity (K)
AMSU-A:			
1	23800 ± 72.5	2 x 125	0.20
2	31400 ± 50	2 x 80	0.27
3	50300 ± 50	2 x 80	0.22
4	52800 ± 105	2 x 190	0.15
5	53596 ± 115	2 x 168	0.15
6	54400 ± 105	2 x 190	0.13
7	54940 ± 105	2 x 190	0.14
8	55500 ± 87.5	2 x 155	0.14
9	57290 ± 87.5	2 x 155	0.20
10	57290 ± 217	2 x 77	0.22
11	$\nu_{11^-} \pm 48$, $\nu_{13^-} \pm 48$	4 x 35	0.24
12	$\nu_{11^-} \pm 22$, $\nu_{13^-} \pm 22$	4 x 15	0.35
13	$\nu_{11^-} \pm 10$, $\nu_{13^-} \pm 10$	4 x 8	0.47
14	$\nu_{11^-} \pm 4.5$, $\nu_{13^-} \pm 4.5$	4 x 3	0.78
15	89000 ± 1000	2 x 1000	0.11
AMSU-B:			
16	89000 ± 900	2 x 1000	0.37
17	150000 ± 900	2 x 1000	0.84
18	183310 ± 1000	2 x 500	1.06
19	183310 ± 3000	2 x 1000	0.70
20	183310 ± 7000	2 x 2000	0.60

Note: ν_{11^-} = 57612.48 MHz, ν_{13^-} = 56968.21 MHz.

Manuscript received September 18, 2000; revised September 8, 2001. This work was supported by NASA Contract NAS5-31 376.

P. W. Rosenkranz is with the Research Laboratory of Electronics, Massachusetts Institute of Technology, Cambridge, MA 02139-4307 USA (e-mail: pwr@mit.edu).

Publisher Item Identifier S 0196-2892(01)10400-6.

0196–2892/00$10.00 © 2001 IEEE

II. Forward Model

A. Radiative Transfer Calculations

Planck's equation for radiant intensity is a nonlinear function of temperature. For microwave frequencies, however, the physical temperatures encountered in the earth's atmosphere lie at the high-temperature asymptote of this function. Hence, brightness temperature can be used as a surrogate for radiance in the equation of radiative transfer with an accuracy of a few hundredths of a Kelvin. The only exception to this statement occurs with the cosmic background, which must be assigned an effective brightness temperature at frequency ν of [5]

$$\Theta_C = (h\nu/2k)(e^{h\nu/kTc}+1)(e^{h\nu/kTc}-1)^{-1} \tag{1}$$

instead of its actual temperature $T_c = 2.73$ K, in order to linearize Planck's function.

The equation of radiative transfer is written in the form

$$\Theta = \Theta_{\text{direct}} + \tau[\Theta_S + \Theta_{\text{sky}}(1-\Theta_S/T_S)] \tag{2}$$

where Θ is the brightness temperature emitted from the top of the atmosphere, τ is the one-way transmittance of the atmosphere, Θ_{direct} is the component of brightness temperature emitted from the atmosphere on a direct path to space, T_s is the surface temperature, Θ_s is the surface brightness temperature, and Θ_{sky} is the sky brightness temperature (including the attenuated cosmic contribution) as it would be observed from the surface. Atmospheric transmittance is computed with the rapid algorithm described in [6], [7]. The form of (2) allows separation of the estimation of surface brightness from estimation of temperature, as discussed in the next section.

Based on experience with NOAA-15 data, Θ_{sky} is computed for a path length (or opacity) equal to 1.15 times the path length for specular reflection (1.10 for channels 4–14). This empirical adjustment accounts approximately for the effect of ocean surface nonspecularity, and is roughly consistent in magnitude with the calculations in [8]. For higher-emissivity land surfaces, the adjustment has a negligible effect.

In addition to computing brightness temperatures from the estimated atmospheric and surface parameters at each iteration step, the forward model also must provide derivatives of the brightness temperatures with respect to those parameters. The derivatives corresponding to atmospheric temperature are given by

$$\partial\Theta/\partial T = K + G\partial\kappa/\partial T \tag{3}$$

where K is equal to the temperature weighting function as defined in [9] integrated over an atmospheric layer at temperature T having opacity $\kappa, G = \partial\Theta/\partial\kappa$, and $\partial\kappa/\partial T$ is computed by the rapid transmittance algorithm. G is equal to the integral over an atmospheric layer of the function $G(h)$ defined in [9]. The second term on the right side of (3) is a small correction to the temperature weighting function. The derivatives corresponding to T_S are obtained by partial differentiation of (2):

$$\partial\Theta/\partial T_S = \tau\Theta_{\text{sky}}\Theta_S T_S^{-2} \tag{4}$$

The dependence on T_S is nonlinear because Θ_S is considered to be an independent input, from the moisture/surface brightness algorithm described below.

B. Surface Brightness Model

The model for the surface combines an *a priori* emissivity of the surface type with an analytic function which allows the retrieval to adapt the surface brightness temperature to the data. The surface brightness temperature spectrum Θ_s is modeled as

$$\Theta_s = T_s\varepsilon_o + \frac{R_oT_o + R(\nu)T_\infty}{R_o + R(\nu)} \tag{5}$$

where ε_o is a preliminary estimate of surface emissivity, and R_o and $R(\nu)$ are defined as

$$R_o = (\nu_o/31.4\,\text{GHz})^S \tag{6}$$

$$R(\nu) = (\nu/31.4\,\text{GHz})^S. \tag{7}$$

The second term in (5) is a smooth four-parameter function of frequency [10] which allows for effects such as ocean surface roughness, errors in the dielectric constant model, mis-classification of the surface, or errors in the land fraction within a footprint. T_o, T_∞, ν_o and s are parameters defining the curve. The retrieval algorithm fixes s at 1.2 over land or mixed land/water, or 3 over ocean, and treats R_o, T_o and T_∞ as uncorrelated free parameters for which it solves. The derivatives of brightness temperature with respect to the surface parameters are obtained from (2) and (5), using the chain rule for differentiation.

For the data considered in this paper, the only surface types are land and ocean. For land, $\varepsilon_o = 0.95$. For ocean, ε_o is calculated by a second-order polynomial function of temperature with coefficients fitted to the emissivity of a flat surface viewed in the polarization of the radiometers, which rotates with scan angle. A separate set of these coefficients was precomputed for each incidence angle and frequency. The model in [11] was used for seawater dielectric constant at 23.8 and 31.4 GHz, and the model in [12] was used at higher frequencies. For future use with data from the Aqua spacecraft instruments, mixtures of land and water within a footprint will be determined from a coastline map and interpolated between the corresponding emissivities. Classifications for ice and snow are under development.

C. Atmospheric Moisture and Condensation Model

Brightness temperatures at the AMSU-B frequencies depend on the vertical profile of atmospheric opacity relative to temperature, but do not by themselves distinguish, at any given altitude, between opacity due to water vapor and opacity due to liquid water. However, the physics of water vapor condensation add some *a priori* information or constraints. Cloud coverage is parameterized as in the stratiform condensation model of [13], where a relative humidity threshold determines the onset of condensation. Although the water vapor profile is saturated within the cloudy part of the field of view, it is assumed that the condensation process is not spatially resolved, hence the threshold is less than 100% relative humidity. Currently, the threshold is set to 85%.

In the condensation model, the vapor and cloud liquid water density profiles are both linked to a single parameter H, as il-

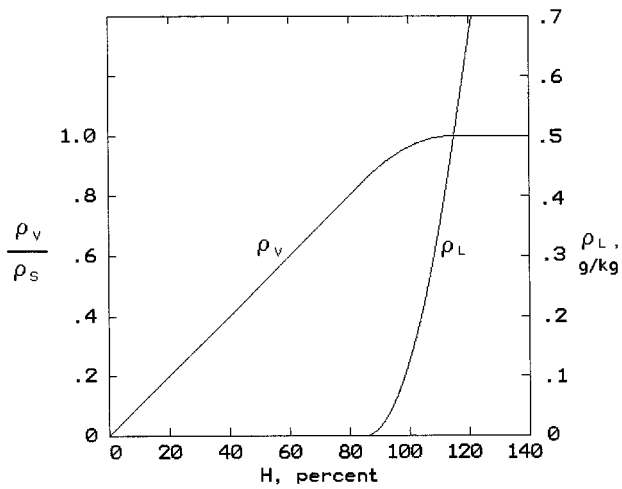

Fig. 1. Water vapor (ρ_v) and cloud liquid (ρ_L) mixing ratios as functions of $H; \rho_s =$ saturation vapor mixing ratio.

lustrated in Fig. 1. When $H \leq 85$ percent, H is equal to relative humidity; in the range 85 to 115, H changes from a water-vapor variable to liquid-water, and values of $H > 115$ increase liquid water while the vapor remains at saturation. Because convergence, to be discussed later, is determined from the brightness temperature residuals, which in turn are computed using the vapor and liquid column densities, the role of H in this algorithm is only to introduce the *a priori* statistics and constraints. The average vapor density in the field of view is related to H by

$$\rho_v = \begin{cases} \rho_s H/100 & \text{if } H \leq 85 \\ \rho_s[0.85 + 0.15(2b - b^2)] & \text{if } 85 < H < 115 \\ \rho_s & \text{if } H \geq 115 \end{cases} \quad (8)$$

and the liquid water density averaged over the field of view is calculated as

$$\rho_L = \begin{cases} 0 & \text{if } H \leq 85 \\ C_L b^2 & \text{if } 85 < H < 115 \\ C_L(2b - 1) & \text{if } H \geq 115 \end{cases} \quad (9)$$

In the previous equation, $b = (H - 85)/30, \rho_s$ is the saturation value of vapor density, and C_L is a coefficient equivalent to a mass mixing ratio of 0.5 g liquid/kg air. The saturation vapor density is computed from the temperature profile. Saturation is calculated with respect to liquid water (by extrapolation) even when the temperature is below 273 K. Thus, this model will allow supercooled liquid water clouds and water vapor greater than the saturation value over ice (but not greater than ρ_s).

The derivative of brightness temperature with respect to H will be used in the retrieval and is given by

$$\partial\Theta/\partial H = G \cdot (\partial\kappa/\partial\rho_v \cdot \partial\rho_v/\partial H + \partial\kappa/\partial\rho_L \cdot \partial\rho_L/\partial H) \quad (10)$$

in which $G = \partial\Theta/\partial\kappa$, where κ represents the opacity of the layer. The derivatives $\partial\kappa/\partial\rho_v$ and $\partial\kappa/\partial\rho_L$ are computed with the rapid transmittance algorithm [7] using the estimated temperature and moisture profiles. The latter derivative is calculated in the small-droplet (Rayleigh) approximation; hence, it is valid only in nonprecipitating cloud situations. Differentiation of (8) and (9) yields $\partial\rho_v/\partial H$ and $\partial\rho_L/\partial H$. The transitions at $H = 85$ and 115 have continuous first derivatives.

III. Solution Method

A. Outline

Retrievals are done at AMSU-A resolution, hence, the AMSU-B measurements are weighted averages over 3×3 spatial arrays that approximate the AMSU-A footprint, nominally 50 km diameter near nadir. The input vector of measured brightness temperatures is accompanied by an input validity vector whose elements are either one or zero. This provides a way of handling missing or bad data. Because the design of the algorithm is motivated by future applications to Aqua data, channel 16 is not used. That channel will not be included on the Aqua instruments. The principal steps in the retrieval algorithm are the following.

1) Based on location and month, choose an *a priori* temperature profile $\hat{T}_o$. At present the *a priori* relative humidity is global. Also calculate the geomagnetic field, which has a minor effect on the transmittance of channel 14.
2) Using location or other criteria, classify the surface as discussed in Section II-B. Compute an *a priori* surface brightness temperature for this class. This will depend on surface temperature, by (5).
3) Test for convergence of channels 1, 2, 3, 15, and 17–20 brightness temperatures. If not converged, update the H profile and the surface brightness temperature spectrum using these channels.
4) Test for convergence of channels 4–14. If not converged, update the temperature profile using these channels.
5) Return to step 2 if convergence did not occur in step 4; else to step 3 if convergence did not occur in step 3; else exit.

Steps 3 and 4 are described in greater detail in the following sections.

B. Estimation of Surface Brightness and Atmospheric Moisture

The H profile and the three surface brightness parameters R_o, T_o and T_∞ are concatenated into a vector P. The cost function to be minimized is [18]

$$(\hat{P} - \hat{P}_o)^t \mathbf{S}_P^{-1} (\hat{P} - \hat{P}_o) + (\Theta^* - \Theta)^t \mathbf{S}_e^{-1} (\Theta^* - \Theta). \quad (11)$$

In the previous equation, $\hat{P}$ is the estimate of $P, \hat{P}_o$ is the *a priori* mean value of P and $\mathbf{S}_p$ is its covariance matrix with respect to $\hat{P}_o, \Theta^*$ is a vector containing the measured brightness temperatures of channels 1–3, 15, and 17–20, $\mathbf{S}_e$ is their error covariance matrix, and Θ is a brightness temperature vector computed at each iteration from the current estimated values of temperature, moisture, and surface brightness, using the forward model. Superscript t indicates the transpose.

Given the previous estimate $\hat{P}_{n-1}$ (which is $\hat{P}_o$ on the first iteration), the next estimate of P is obtained by Newtonian iteration [21], except that Eyre's [18] method of damping is used to avoid large relative humidity increments because of the nonlinearity of the problem

$$\hat{P}_n = \hat{P}_{n-1} - \delta[\hat{P}_{n-1} - \hat{P}_o] + \delta \mathbf{S}_P \mathbf{W}_P^t X_P \quad (12)$$

in which X_P is the solution vector to

$$\left[\mathbf{W}_P\delta\mathbf{S}_P\mathbf{W}_P^t+\mathbf{S}_e\right]X_P=\Theta^*-\Theta-\Theta'+\mathbf{W}_P\delta[\hat{P}_{n-1}-\hat{P}_o] \tag{13}$$

where Θ' is a possible correction (presently zero) to adjust for transmittance-model errors, and $\mathbf{W}_p$ is a Jacobian matrix (matrix of derivatives of Θ with respect to P), which is computed for the state represented by $\hat{P}_{n-1}$ (the forward model is assumed to be linearizable within the retrieval error space, which is generally more compact than the *a priori* ensemble.) The damping factor is as in (14), shown at the bottom of the page. Here, δ is a scalar rather than a matrix as in [18].

The parts of $\hat{P}_o$ and $\mathbf{S}_p$ corresponding to relative humidity were calculated from the TIGR profile ensemble [22]. For the surface parts, it is necessary to postulate statistics based on physical considerations and previously observed ranges of variation. Mean values are set to

$$\langle R_o\rangle=3.5\,(\text{land or mixed}),\quad\text{or}\quad 2.1\,(\text{water}) \tag{15a}$$
$$\langle T_o\rangle=0 \tag{15b}$$
$$\langle T_\infty\rangle=0 \tag{15c}$$

and variances are set to

$$S_{R_o}=2.25 \tag{16a}$$
$$S_{T_o}\,(\text{Kelvin})^2=100\,(\text{land})\quad\text{or}\quad 9\,(\text{water}) \tag{16b}$$
$$S_{T_\infty}\,(\text{Kelvin})^2=100\,(\text{land})\quad\text{or}\quad 25\,(\text{water}). \tag{16c}$$

For the moisture channels, the measurement error covariance $\mathbf{S}_e$ is the sum of contributions due to instrument noise (see Table I) plus a diagonal error of (1.5 K)^2, which approximately represents errors in Θ resulting from errors in the temperature profile retrieval.

After update of $\hat{P}$ by (12), the water vapor and liquid water profiles are computed from (8) and (9), and surface brightness is computed for both window and sounding frequencies from (5), using the new estimate. If the estimated vapor mixing ratio at any level is less than 10^{-3} g/kg, it is set to that minimum value.

C. Estimation of the Temperature Profile

Although done separately in step 4 (see Section III-A), the estimation of temperature uses essentially the same equations as Section III-B, but with T replacing P everywhere and with no damping ($\delta=1$). The atmospheric temperature vector is augmented by T_S, which is considered to be distinct from the air temperature near the surface. A cost function of the form (11), with P replaced by T is to be minimized separately for the temperature profile. Given an existing estimate $\hat{T}_{n-1}$, the next estimated profile is determined from a vector Θ^* of observed brightness temperatures for channels 4–14. However, the updated surface temperature is not allowed to become less than the estimated surface brightness temperature $\hat{\Theta}_s$. In (12)–(13), $\mathbf{W}_p$ is replaced by $\mathbf{W}_T$, the Jacobian matrix of derivatives of Θ with respect to T given by (3)–(4), evaluated at $\hat{T}_{n-1}$. The error covariance matrix $\mathbf{S}_e$ includes uncertainties due to surface brightness, water vapor, liquid water, and the instrument noise. The covariance of the atmospheric temperature vector was computed from the TIGR ensemble [22]. To account for differences between T_S and the air temperature near the surface (T_{1013}), the variance of T_S is set to a value 16 K^2 larger than the variance of T_{1013}, but its mean and covariances with other levels are equal to those of T_{1013}. Hence, the correlation coefficient of T_s with other levels is smaller than that of T_{1013} with those levels.

D. Convergence Tests

Convergence is tested separately for the temperature channels in step 4 and for the moisture/surface channels in step 3. Iteration of either step is suspended when one of the following conditions is met: 1) the computed brightness temperature vector Θ meets the noise closure criterion

$$\sum_{i=1}^{N_B}[\Theta_i^*-\Theta_i-\Theta_i']^2\Delta T_i^{-2}\le N_B \tag{17}$$

where ΔT_i is the instrument noise (not the total measurement error) on channel i and N_B is the number of valid elements in Θ^*; 2) when successive computations of the left side of (17) change by less than 1% for the temperature channels or 2% for the moisture/surface channels; or 3) when the number of iterations exceeds a preset limit, currently 12 for the temperature channels and 16 for the moisture/surface channels. Typically, iteration of the temperature profile ceases after one or two iterations, but the moisture profile often requires six or more iterations.

IV. Results With NOAA-15 Data

NOAA-15 data was corrected for contributions from antenna sidelobes using coefficients given by Mo [3] and T. Hewison (private communication, 1998). In Figs. 2 and 3, temperature and dewpoint profiles retrieved from the satellite data are compared with nearby radiosonde measurements. The *a priori* profiles used by the retrieval are also shown in the figures. In both cases the satellite footprint was over land. As expected, the retrieved profiles are fairly smooth curves, without the fine vertical structure of the radiosonde profiles. With these profiles, the highest water-vapor weighting function (channel 18) peaks between 300 and 500 hPa. Consequently the dewpoint errors are larger at higher altitudes. In Fig. 2, the near coincidence of the radiosonde's temperature and dewpoint near the surface indicates possible fog and cloud. The retrieval algorithm places

$$\delta=\begin{cases}1 & \text{if } (\Theta_i^*-\Theta_i-\Theta_i')\le 10\text{ K for all channels } i,\text{ or if the iteration number is }>10\\ 0.1 & \text{otherwise.}\end{cases} \tag{14}$$

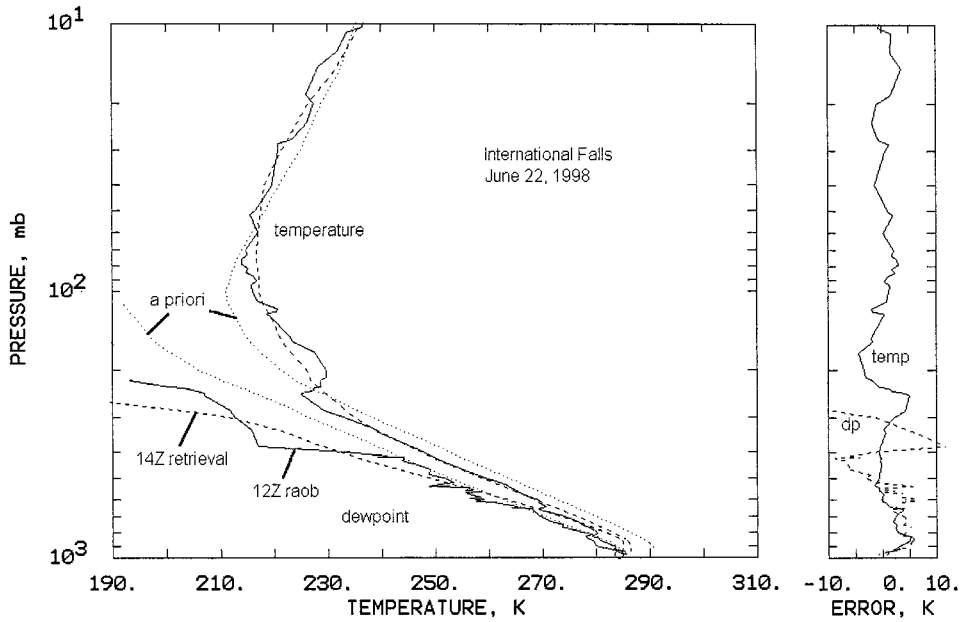

Fig. 2. Retrieval versus radiosonde profiles at International Falls, MN. The circle is retrieved surface temperature.

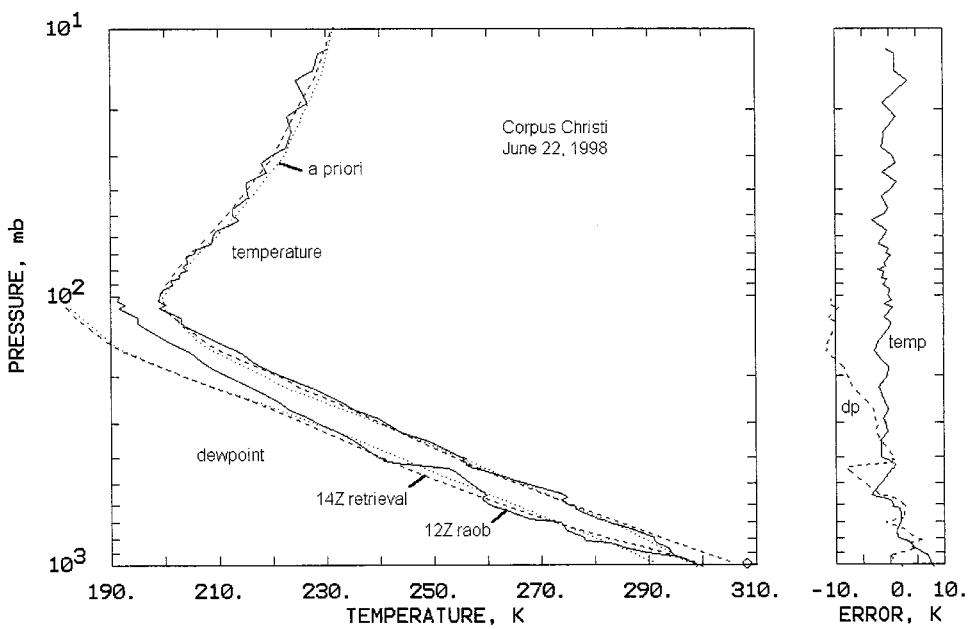

Fig. 3. Retrieval versus radiosonde profiles at Corpus Christi, TX. The circle is retrieved surface temperature.

cloud liquid water between 750 hPa and the surface (using the 85% relative humidity threshold). The radiosonde data in Fig. 3 also indicate fog or cloud between 925 hPa and the surface, but in this case, liquid water was not retrieved because the retrieved temperature within this pressure range is $\sim$5 K too high. Surface observations at the time of the satellite overpass were overcast clouds at 1500 ft (930 hPA) for International Falls, MN, and a few clouds at 1700 ft (965 hPa) for Corpus Christi, TX.

Fig. 4 displays retrieved parameters along a satellite track over the eastern Pacific Ocean. In the top row, integrated liquid water is displayed in the leftmost swath, integrated water vapor and mixing ratio at four different levels in the second through sixth swaths. As one moves upward in the atmosphere, the moisture associated with the intertropical convergence zone becomes more sharply peaked, indicating the presence of a small number of areas with relatively strong convection. The climatological variation of temperature at different levels is reflected in the temperature retrievals in swaths 7–16. An interesting feature is the wave activity visible at the 5 to 20 hPa levels, at the edge of the South Polar vortex. High-latitude temperature waves have also been observed by Wu and Waters [23], [24] and by Eckermann and Preusse [25], who attributed those waves to amplification of weak background gravity-wave activity due to the temperature structure of the winter polar stratosphere.

The three swaths on the top right side of Fig. 4 display the surface brightness parameters R_o, T_o, and T_∞. The last exhibits el-

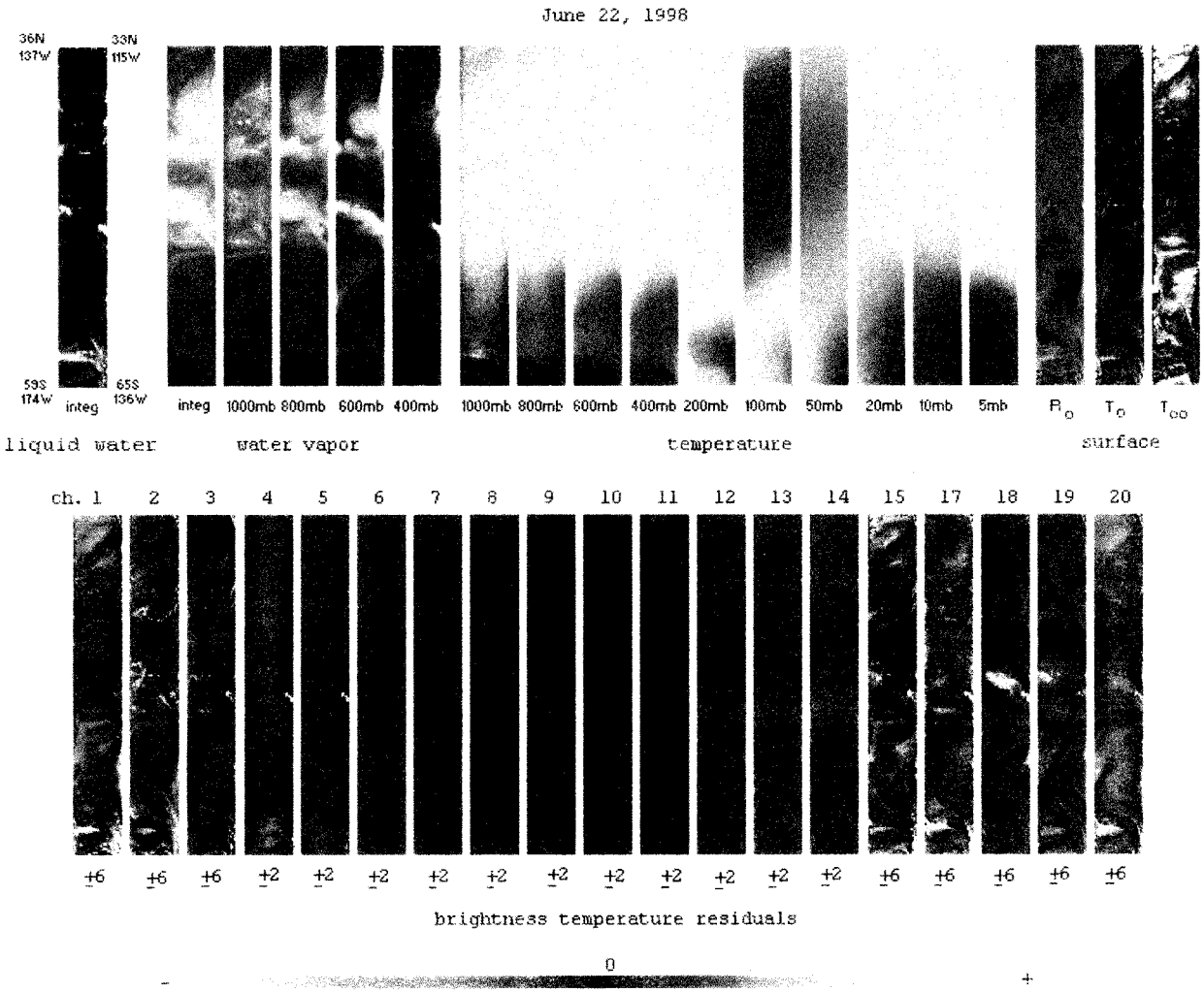

Fig. 4. (Top) Retrieved atmospheric and surface parameters on June 22, 1998: integrated liquid water (0–0.5 kg/m^2); integrated water vapor (0–70 kg/m^2); vapor mixing ratio at four levels (0–30, 0–20, 0–8, 0–3 g/kg). The temperature scales have a range of 45 K from black to white: R_o (0–7), T_o (± 20 K), T_∞ (± 20 K). (Bottom) brightness temperature residuals (K) (note the different scale for channels 4–14).

evated values over two regions, one near the top and another $1/4$ of the way from the bottom of the swath. This could be caused by sea state or possibly by cloud liquid water missed by the condensation model. With the single-polarization AMSU-A/B radiometers, these two effects are difficult to disentangle.

The bottom row of Fig. 4 contains the residuals (measured minus computed brightness temperature) for the 19 channels used in the retrieval algorithm. The largest residuals (for example, near the bottom of the swath in channels 1, 2, 17, and 20) are associated with high values of liquid water, which suggests that precipitation is present there. These large residuals occur because the radiative transfer calculation does not include scattering due to the larger drop sizes (liquid or ice) encountered in raining clouds. Retrievals with such large residuals would normally not be used. Elsewhere in Fig. 4, brightness-temperature residuals in the range of ± 2 K to ± 3 K are seen in areas where T_∞ also has large values. The fact that residuals are large compared to instrument noise indicates that the forward model does not provide adequate degrees of freedom there, possibly because the assumed *a priori* statistics are not representative, or possibly due to inhomogenieties such as unresolved clouds within the instrument footprint.

If the correction described in Section II-A for surface nonspecularity were omitted, then the residuals in channel 3 would be considerably larger over ocean, typically 3–4 K. The reason that this effect becomes noticeable at 50 GHz is that in the absence of the 15% correction to opacity on the specular reflected path, the retrieval algorithm can compensate at most of the window and water-vapor frequencies by an increase of $\sim$5% in retrieved water vapor. However, channel 3 is unique among the window channels in that opacity due to oxygen is greater than the opacity due to the water-vapor continuum.

Future development of this retrieval algorithm will be directed toward improvements in the surface model, treatment of a larger variety of surfaces (e.g., [26]), and the incorporation of precipitation flags and/or corrections [27].

ACKNOWLEDGMENT

The author wishes to thank D. H. Staelin for helpful comments on the manuscript, S. English for providing a sea surface emissivity model, and E. Wack and P. Piraino for assistance in obtaining data.

REFERENCES

[1] T. Mo, "Prelaunch calibration of the advanced microwave sounding unit—A for NOAA-K," *IEEE Trans. Microwave Theory Tech.*, vol. 44, pp. 1460–1469, Dec. 1996.

[2] R. W. Saunders, T. J. Hewison, N. C. Atkinson, and S. J. Stringer, "The radiometric characterization of AMSU-B," *IEEE Trans. Microwave Theory Tech.*, vol. 43, pp. 760–771, May 1995.

[3] T. Mo, "AMSU-A antenna pattern corrections," *IEEE Trans. Geosci. Remote Sensing*, vol. 37, pp. 103–112, 1999.

[4] T. J. Hewison and R. Saunders, "Measurements of the AMSU-B antenna pattern," *IEEE Trans. Geosci. Remote Sensing*, vol. 34, pp. 405–412, Mar. 1996.

[5] M. A. Janssen, Ed., *Atmospheric Remote Sensing by Microwave Radiometry*. New York, NY: Wiley, 1993, ch. 1.

[6] P. W. Rosenkranz, "A rapid atmospheric transmittance algorithm for microwave sounding channels," *IEEE Trans. Geosci. Remote Sensing*, vol. 33, pp. 1135–1140, 1995.

[7] ——, "Improved rapid transmittance algorithm for microwave sounding channels," in *1998 IEEE Int. Geoscience and Remote Sensing Symp. Proc.*, 1998, pp. 728–730.

[8] A. Guissard and P. Sobieski, "A simplified radiative transfer equation for application in ocean microwave remote sensing," *Radio Sci.*, vol. 29, pp. 881–894, 1994.

[9] G. Schaerer and T. T. Wilheit, "A passive microwave technique for profiling of atmospheric water vapor," *Radio Sci.*, vol. 14, pp. 371–375, 1979.

[10] N. C. Grody, "Surface identification using satellite microwave radiometers," *IEEE Trans. Geosci. Remote Sensing*, vol. 26, pp. 850–859, 1988.

[11] C. Guillou, W. Ellison, L. Eymard, K. Lamkaouchi, C. Prigent, G. Delbos, G. Balana, and S. A. Boukabara, "Impact of new permittivity measurements on sea surface emissivity modeling in microwaves," *Radio Sci.*, vol. 33, pp. 649–667, 1998.

[12] K. Lamkaouchi, G. Balana, and W. Ellison, "New Permittivity Data for Sea Water (30–100 GHz),", ESA Report 11 197/94/NL/CN, 1997.

[13] H. Sundqvist, E. Berge, and J. E. Kristjansson, "Condensation and cloud studies with a mesoscale numerical prediction model," *Mon. Wea. Rev.*, vol. 117, pp. 1641–1657, 1989.

[14] J. R. Wang and L. A. Chang, "Retrieval of water vapor profiles from microwave radiometric measurements near 90 and 183 GHz," *J. of App. Meteor.*, vol. 29, pp. 1005–1013, 1990.

[15] C. Kuo, D. H. Staelin, and P. W. Rosenkranz, "Statistical iterative scheme for estimating atmospheric relative humidity profiles," *IEEE Trans. Geosci. Remote Sensing*, vol. 32, pp. 254–260, 1994.

[16] T. T. Wilheit, "An algorithm for retrieving water vapor profiles in clear and cloudy atmospheres from 183 GHz radiometric measurements, Simulation studies," *J. App. Meteor.*, vol. 29, pp. 508–515, 1990.

[17] T. T. Wilheit and K. D. Hutchison, "Water vapor profile retrievals from SSM/T-2 data constrained by infrared-based cloud parameters," *Int. J. Remote Sensing*, vol. 18, pp. 3263–3277, 1997.

[18] J. R. Eyre, "Inversion of cloudy satellite sounding radiances by nonlinear optimal estimation. I: Theory and simulation for TOVS," *Q. J. R. Meteorol. Soc.*, vol. 115, pp. 1001–1026, 1989.

[19] M. J. Rieder and G. Kirchengast, "An inversion algorithm for nonlinear retrieval problems extending Bayesian optimal estimation," *Radio Sci.*, vol. 35, pp. 45–56, 2000.

[20] S. English, "Estimation of temperature and humidity profile information from microwave radiances over different surface types," *J. Appl. Meteor.*, vol. 38, pp. 1526–1541, 1999.

[21] C. D. Rodgers, "Retrieval of atmospheric temperature and composition from remote measurements of thermal radiation," *Rev. Geophys. and Space Phys.*, vol. 14, pp. 609–624, 1976.

[22] A. Chedin, N. A. Scott, C. Wahiche, and P. Moulinier, "The improved initialization inversion method: A high resolution physical method for temperature retrievals from the TIROS-N series," *J. Clim. Appl. Meteor.*, vol. 24, pp. 128–143, 1985.

[23] D. L. Wu and J. W. Waters, "Satellite observations of atmospheric variances: A possible indication of gravity waves," *Geophys. Res. Lett.*, vol. 23, pp. 3631–3634, 1996.

[24] ——, "Gravity-wave-scale temperature fluctuations seen by the UARS MLS," *Geophys. Res. Lett.*, vol. 23, pp. 3289–3292, 1996.

[25] S. D. Eckermann and P. Preusse, "Global measurements of stratospheric mountain waves from space," *Science*, vol. 286, pp. 1534–1537, 1999.

[26] N. Grody, F. Weng, and R. Ferraro, "Application of AMSU for obtaining hydrological parameters," in *Microwave Radiometry and Remote Sensing of the Earth's Surface and Atmosphere*, P. Pampaloni and S. Paloscia, Eds: VSP, 2000, ISBN 90-6764-318-1, pp. 339–352.

[27] D. H. Staelin and F. W. Chen, "Precipitation observations near 54 and 183 GHz using the NOAA-15 satellite," *IEEE Trans. Geosci. Remote Sensing*, vol. 38, pp. 2322–2332, Sept. 2000.

Philip W. Rosenkranz (S'68-M'71-SM'84-F'97) received the S.B., S.M., and Ph.D. degrees in electrical engineering from the Massachusetts Institute of Technology (MIT), Cambridge, in 1967, 1968, and 1971, respectively.

He did postdoctoral work at Caltech's Jet Propulsion Laboratory, then in 1973 joined the Research Staff at MIT's Research Laboratory of Electronics, where he is presently a Principal Research Scientist. His field of interest is the interaction of electromagnetic waves with constituents of the terrestrial atmosphere and surface, and remote sensing of geophysical parameters from aircraft and satellites. Examples of this work are theoretical models for absorption in molecular oxygen and water vapor, and studies of hurricane phenomenology, such as the warm core and scattering in rainbands, with microwave radiometers. He is a member of the Science Team for the Atmospheric Infrared Sounder Facility on NASA's Earth Observing System.